Highly Enhanced Gas Adsorption Properties in Vertically Aligned MoS_2 Layers

Soo-Yeon Cho,[†] Seon Joon Kim,[†] Youhan Lee,[†] Jong-Seon Kim,[†] Woo-Bin Jung,[†] Hae-Wook Yoo,[‡] Jihan Kim,[*,†] and Hee-Tae Jung[*,†]

[†]Department of Chemical and Biomolecular Engineering (BK-21 Plus), Korea Advanced Institute of Science and Technology(KAIST), Daejeon 305-701, Korea and [‡]Advanced Technology Agile Development Center, Agency for Defense Development (ADD), Daejeon 305-600, Korea

ABSTRACT In this work, we demonstrate that gas adsorption is significantly higher in edge sites of vertically aligned MoS_2 compared to that of the conventional basal plane exposed MoS_2 films. To compare the effect of the alignment of MoS_2 on the gas adsorption properties, we synthesized three distinct MoS_2 films with different alignment directions ((1) horizontally aligned MoS_2 (basal plane exposed), (2) mixture of horizontally aligned MoS_2 and vertically aligned layers (basal and edge exposed), and (3) vertically aligned MoS_2 (edge exposed)) by using rapid sulfurization method of CVD process. Vertically aligned MoS_2 film shows about 5-fold enhanced sensitivity to NO_2 gas molecules compared to horizontally aligned MoS_2 film. Vertically aligned MoS_2 has superior resistance variation compared to horizontally aligned MoS_2 even with same surface area exposed to identical concentration of gas molecules. We found that electrical response to target gas molecules correlates directly with the density of the exposed edge sites of MoS_2 due to high adsorption of gas molecules onto edge sites of vertically aligned MoS_2. Density functional theory (DFT) calculations corroborate the experimental results as stronger NO_2 binding energies are computed for multiple configurations near the edge sites of MoS_2, which verifies that electrical response to target gas molecules (NO_2) correlates directly with the density of the exposed edge sites of MoS_2 due to high adsorption of gas molecules onto edge sites of vertically aligned MoS_2. We believe that this observation extends to other 2D TMD materials as well as MoS_2 and can be applied to significantly enhance the gas sensor performance in these materials.

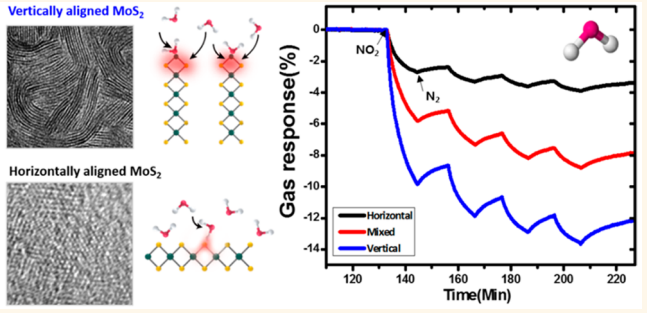

KEYWORDS: MoS_2 · 2D material · chemical vapor deposition · gas adsorption · density functional theory

The prototypical transition metal dichalcogenides (TMD) of molybdenum disulfide (MoS_2) that consists of two-dimensional (2D) molecular layers stacked together by weak interlayer interaction have received tremendous amount of attention in recent years due to their unique thickness-dependent band gap and excellent electrochemical/thermal properties.[1,2] The MoS_2 usually exposes the basal planes as the terminating surface with minimal dangling bonds and roughness because edge sites of MoS_2 possess high surface energies that are hard expose to the outside.[3] This basal plane exposed MoS_2 has been very useful for many applications including field effect transistor (FET), photodetector and sensing device materials, showing high carrier mobility and fast response to stimulation with in-plane transportation.[4−7] Among many applications, MoS_2 used as a gas sensing material is particularly interesting due to the various active sites (sulfur defect, vacancy, and edge sties of MoS_2) for selective molecular adsorption, semiconducting behaviors, high surface-to-bulk atom ratios and high yield preparation of the materials.[8−10] Although many researchers have experimentally and theoretically exploited the unique gas adsorption properties of MoS_2, all of the studies on gas adsorption using MoS_2 relied on the use of a basal plane of the MoS_2 nanostructure, which is relatively easy to expose and prepared by CVD synthesis and chemical exfoliation.

Recently, it was reported that edge sites of nanostructured MoS_2 show much higher chemical catalytic activity compared to the

* Address correspondence to jihankim@kaist.ac.kr, heetae@kaist.ac.kr.

Received for review July 20, 2015 and accepted August 27, 2015.

Published online August 27, 2015
10.1021/acsnano.5b04504

basal plane, which is attributed to the different local stoichiometry of MoS_2 sites found in the two planes.[11] Unlike the basal plane, the vertically aligned MoS_2 is composed of (002) plane of the MoS_2 crystal structure terminated with dominantly exposed molybdenum or sulfur atoms.[12,13] To exploit such novel catalytic properties of the edge sites, various methods including rapid sulfurization method of CVD have been used to synthesize vertically aligned MoS_2 layers.[14−17] Recent studies demonstrate that such MoS_2 nanostructure that exposes their edge sites is not only beneficial for hydrogen evolution reaction (HER)[18] and carbon dioxide reduction reaction,[19] but also provides tunable wettability[20] and strong resonant nonlinear optical susceptibilities allowing direct optical imaging of the MoS_2.[21] Therefore, it is highly anticipated that the gas adsorption behavior of MoS_2 can be significantly affected by the alignment of MoS_2 layers because the edge sites of MoS_2 contain high d-orbital electron density that can induce strong binding interactions between the gas molecules and the MoS_2.

In this work, we first demonstrate the enhancement of gas adsorption properties along the MoS_2 edge sites. We found that the gas sensing capability is strongly influenced by MoS_2 alignment, in which MoS_2 films with three different alignments were prepared by using predeposited Mo seed layers with different thicknesses.[22] Nitrogen dioxide (NO_2) sensing results show that the vertically aligned MoS_2 has superior sensing performance (about 5-fold enhanced sensitivity) compared to the horizontally grown MoS_2. We found that electrical response to target gas molecules correlates directly with the density of the exposed edge sites of MoS_2 due to high adsorption of gas molecules onto edge sites of vertically aligned MoS_2. This was verified by the density functional theory (DFT) calculations, which shows multiple configurations along the edge sites of MoS_2 with stronger NO_2 binding energies. We believe that these results provide clear comparison between gas adsorption properties of the edge and the terrace sites of MoS_2 and can significantly advance MoS_2 based gas sensing performance. A significant step was taken toward solving limitations imposed by previous MoS_2 based gas sensor, which were based mostly on basal plane having low adsorption energy and active sites *via* aligning MoS_2 layer along the vertical direction.

RESULTS AND DISCUSSION

Overall scheme for the fabrication of NO_2 adsorption chemiresistors using CVD grown MoS_2 films with various alignments is displayed in Figure 1. Mo seed layers are deposited on predefined region of SiO_2 deposited Si wafer using electron beam evaporator (Figure 1a,b). The predeposited Mo seed layer is converted to MoS_2 film by rapid sulfurization during CVD process (Figure 1c).[15] A detailed CVD synthesis processing condition is described in Method section and the Supporting Information (Figure S1). To investigate the effect of the MoS_2 alignment on the gas sensing capabilities, we synthesized three distinct MoS_2 films: (i) horizontally aligned MoS_2 (basal plane exposed), (ii) horizontally aligned MoS_2 with regions of vertically aligned layers (basal and edge exposed), and (iii) vertically aligned MoS_2 exposing their edge sites in a maximized manner using a rapid sulfurization method in single CVD process. MoS_2 films with different layer alignments were prepared by using predeposited Mo seed layers with different thicknesses (1, 5, and 15 nm), as reported recently.[22] Growth direction of MoS_2 films is varied from horizontal to vertical direction with respect to substrate surface as Mo seed layer thickness increases from 1 to 15 nm. A 100 nm-thick gold electrode with a Ti adhesion layer is then deposited on the resulting MoS_2 layers using electron beam evaporator with a predetermined shadow metal mask (Figure 1d). Finally, gas adsorption behavior is characterized with resistance measurement in reaction chamber connected with data acquisition module and gas control system (Figure 1e). The detail gas delivery system, which is fabricated in-house, is shown in the Supporting Information (Figure S2).

Photo images of the chemiresistors fabricated with as-synthesized MoS_2 film channels with three different Mo seed layers thickness (1, 5, and 15 nm from left) are shown in Figure 1f. Color evolution from blue (1 nm) to yellow (15 nm) indicates that synthesized MoS_2 films have different Mo seed layer thicknesses. Optical microscope (OM) images demonstrate that 100 μm width MoS_2 film channel is well connected between Au electrodes (Figure 1g). Atomic force microscopy (AFM) was used to investigate surface roughness of synthesized MoS_2 films (Figure S3). Although the vertically aligned MoS_2 films with 15 nm-thick seed layer is slightly rougher (<2 nm) than that of the horizontally grown MoS_2 films with 1 nm-thick seed layer (<0.2 nm), both films show conformal and uniform surfaces suggesting that the effect of surface roughness on gas adsorption is negligible.

To identify the alignment of MoS_2 grown on the various Mo seed layer thicknesses, we conducted X-ray diffraction (XRD) and Raman spectroscopy. XRD patterns of the synthesized MoS_2 films show two clear crystal peaks at $2\theta = 32°$ and $2\theta = 33°$, representing (100) crystal peak of MoS_2 (MoS_2, JCPDS #.37-1492) and Si substrate peak, respectively (Figure 2a). The intensity of the (100) peak drastically increases with increase of thickness of Mo seed layer from 1 to 15 nm. Because the (100) plane represents the edge plane of the MoS_2 crystal structure vertical to basal plane,[12,13] the peak intensity increase of the (100) plane indicates that edge sites of MoS_2 are fully exposed with larger Mo seed layer thickness. The relationship between MoS_2 layer alignment and Mo seed layer thickness is further

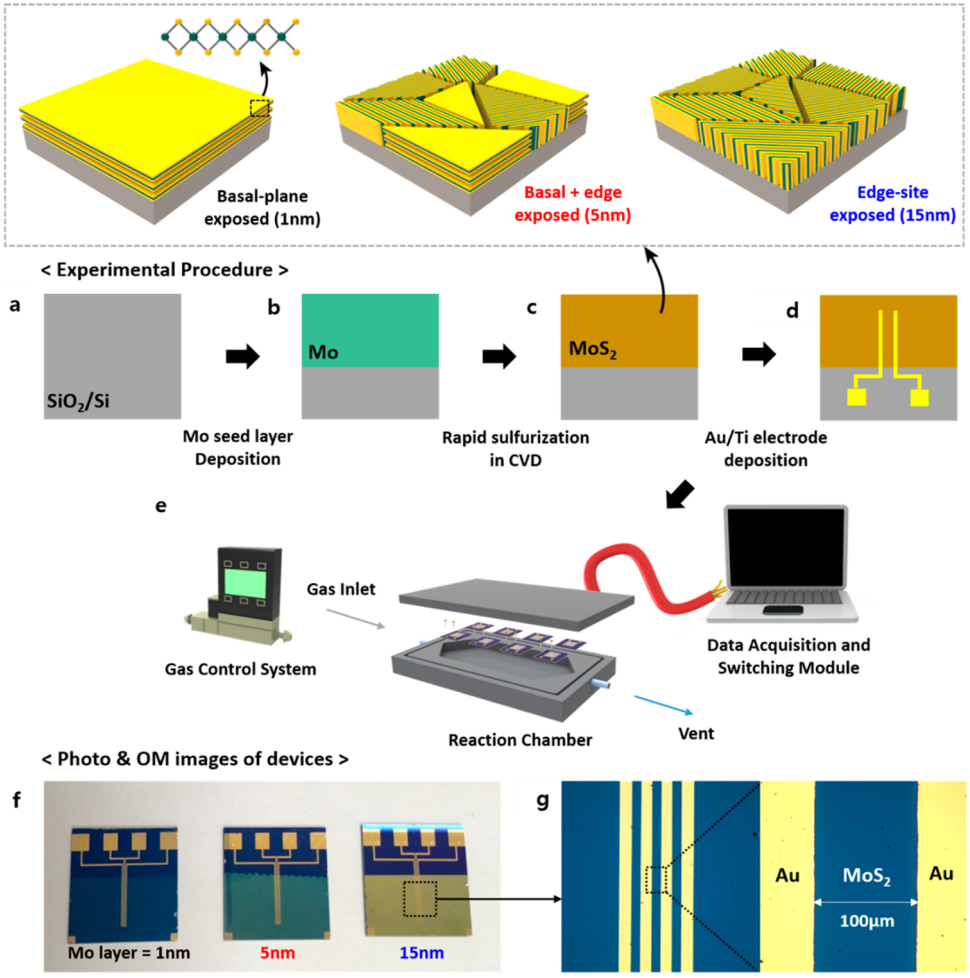

Figure 1. Schematic illustrations of the fabrication of NO_2 adsorption chemiresistors based on CVD grown MoS_2 films with different layers alignment. (a and b) Mo seed layers are deposited on predefined region of SiO_2 deposited Si wafer using electron beam evaporator. (c) The predeposited Mo seed layers are converted to MoS_2 films by rapid sulfurization method during CVD process. Growth direction of MoS_2 films is changed from horizontal to vertical alignment as Mo seed layer thickness increases. (d) Au/Ti electrode is deposited on the resulting MoS_2 layers using electron beam evaporator with a predetermined shadow metal mask. (e) Gas adsorption behavior is characterized with resistance measurement in reaction chamber connected with data acquisition module and gas control system. (f and g) Photo and OM images of the chemiresistors.

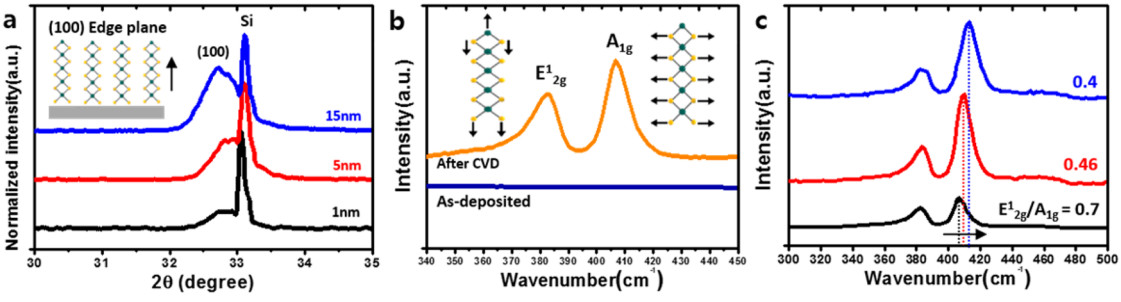

Figure 2. (a) XRD spectra show that intensity of the (100) peak drastically increases with increase of thickness of Mo seed layer from 1 to 15 nm indicating that edge sites of MoS_2 are fully exposed with increase of the Mo seed layer thickness. (b) Raman spectroscopy shows that two representative E^1_{2g} and A_{1g} vibration peaks are formed after CVD process demonstrating Mo seed layer is finely synthesized to MoS_2 films. (c) Intensity ratio of E^1_{2g}/A_{1g} decreases with increasing Mo seed layer thickness reflecting the dominantly exposed MoS_2 edge sites.

clarified by Raman spectroscopy (Figure 2b). Two representative Raman absorption peaks at ~383 and ~408 cm^{-1} are ascribed to the E^1_{2g} and A_{1g} vibration of the MoS_2 film, respectively. Because E^1_{2g} reflects in-plane vibration and A_{1g} reflects out-of-plane vibration of MoS_2 bonding, it is confirmed that Mo seed layer is

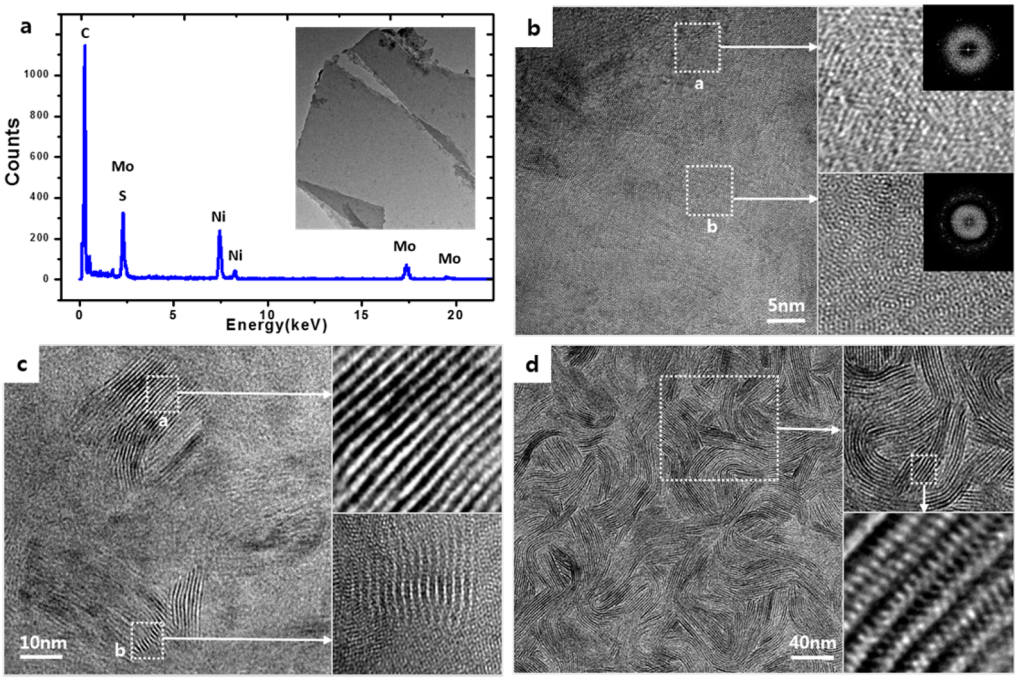

Figure 3. TEM characterizations of MoS_2 films grown with (b) 1 nm, (c) 5 nm, and (d) 15 nm predeposited Mo precursor. (a) EDX spectrum of TEM image indicates that clear chemical compositions of Mo and S, and no other element on synthesized MoS_2. As the Mo seed layer thickness increases to 15 nm, a morphological transition occurs from horizontally to vertically grown MoS_2 layers. With these TEM characterizations, it is clearly confirmed that MoS_2 films with three different layer alignments are well synthesized with single CVD process.

finely synthesized into MoS_2 films after rapid sulfurization of the CVD process. It is noticeable that the intensity ratio of E^1_{2g}/A_{1g} (0.7, 0.46, and 0.4) decreases with increasing Mo seed layer thickness (1, 5, and 15 nm, respectively) (Figure 2c). This is attributed to pronounced A_{1g} (out-of-plane vibration) over E^1_{2g} (in-plane vibration), reflecting the dominantly exposed MoS_2 edge site.[22] In addition, upward shifts of A_{1g} with increasing Mo layer are observed (black arrow), which indicates that vertically aligned MoS_2 layer has larger number of van der Waals (vdW) layers' interactions within large area than horizontally aligned MoS_2 layer.[23]

Transmission electron microscopy (TEM) images further confirm the change of alignment direction of MoS_2 layer grown on the various Mo seed layer thicknesses. Energy dispersive X-ray (EDX) spectrum of TEM clearly exhibits Mo, S, Ni and carbon peaks, in which Ni and carbon peaks come from carbon coated nickel TEM grid used to support MoS_2 layer for TEM analysis. Therefore, the MoS_2 films are well synthesized by CVD process (Figure 3a). The inset TEM image represents CVD grown MoS_2 film with 5 nm seed layer uniformly supported on Ni TEM grid. Figure 3b–d represents TEM images of MoS_2 films grown on three different Mo seed layer thicknesses (1, 5, and 15 nm). The MoS_2 film grown with 1 nm Mo seed layer shows horizontally aligned MoS_2 over large-areas (Figure 3b). High-resolution TEM (HRTEM) image and selective area electron diffraction (SAED) pattern of the horizontally aligned MoS_2 show that stacking of MoS_2 is different over the substrate: (i) grain with precisely stacked MoS_2 few layers showing hexagonal lattice symmetry (box a) and (ii) grain with vertically mismatched MoS_2 few layer revealed by its typical Moiré fringes (box b). When Mo seed layer thickness increased to 5 nm, vertically aligned MoS_2 started to form with horizontally grown MoS_2 film (Figure 3c). In some regions (box a), MoS_2 layer is fully vertical with 10 nm long and several tens of nanometers wide as revealed by black and white stripe-like image showing clear edge configuration ordered in single direction. In other region, MoS_2 layer just started to grow vertically within horizontally aligned MoS_2 layers (box b). For 15 nm thick Mo seed layers, MoS_2 films are aligned to fully vertical (Figure 3d). The typical TEM image of MoS_2 grown on 15 nm seed layer shows large area, edge exposed MoS_2 films with densely packed, stripe-like grains. HRTEM images clearly demonstrate unique edge atomic structure of MoS_2 ordered in the S–Mo–S sequence to form each layers, as the Mo atoms are heavier and thus appear brighter. Therefore, horizontal and vertical alignments of MoS_2 are generated by controlling Mo seed layer thickness.

Gas adsorption properties depending on the alignment of MoS_2 films were investigated by resistance variation measurements to NO_2 gas exposure (Figure 4). First, we measured the resistance of each film with two-probe electrode to verify the effect of the growth orientations on the electrical transportation properties

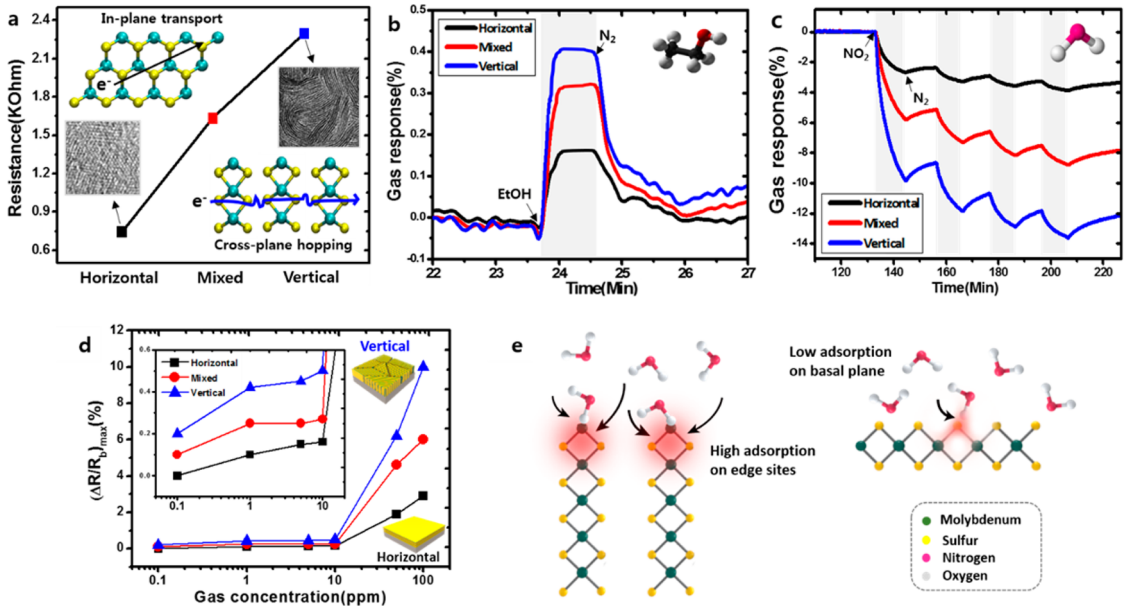

Figure 4. Gas adsorption properties of synthesized MoS_2 films with various layers alignment. (a) Vertically aligned MoS_2 films show higher resistance due to cross-plane hopping of carriers. Resistance changes of synthesized MoS_2 films upon adsorption of (b) 1000 ppm ethanol (C_2H_5OH) and (c) 100 ppm of NO_2 gas demonstrate that edge sites of MoS_2 show superior gas adsorption properties than basal plane. (d) Resistance response upon exposure to NO_2 gas with concentrations ranging from 0.1 to 100 ppm. (e) Schematic illustration of gas adsorption mechanism on edge sites and basal plane of MoS_2.

of MoS_2. Figure 4a shows that resistance of the film is drastically increased as the alignment of MoS_2 layers changes from horizontal to vertical direction. This is because the carrier transport is dominated in the region of vertically aligned layers by a cross-plane hopping process, in which carriers must travel through a large number of vdW gaps as contrast to the in-plane transport of basal plane.[22] Resistance changes of MoS_2 films upon adsorption of 1000 ppm (ppm) ethanol (C_2H_5OH) and 100 ppm of NO_2 gas molecules in room temperature (RT) operation are shown in Figure 4, panels b and c, respectively. When ethanol gas is exposed onto films, vertically aligned MoS_2 shows about 4-times higher positive gas response ($\Delta R/R_b$) than horizontally aligned MoS_2 films. Here, R_b and ΔR represent the baseline resistance of the MoS_2 films and the change in resistance after exposure to gas molecules, respectively. With nitrogen (N_2) gas purging, the resistance of the films is mostly recovered to baseline resistance. When NO_2 molecules are injected, the vertically aligned MoS_2 films also shows about 5-times higher negative resistance variation than horizontally aligned MoS_2 films. When NO_2 gas is adsorbed on MoS_2 films, it is relatively hard to recover to baseline resistance by N_2 purging compared to ethanol adsorption due to high adsorption energy of NO_2 molecules. The dangling bonds of edge sites of vertically aligned MoS_2 layers adsorb the target analytes inducing chemisorption process formed by charge transfer between gas molecules and MoS_2 layers.[7,10] This chemisorption process causes the significant electrical resistance variation of the MoS_2 channel. It is noticeable that all MoS_2 films synthesized in this study show p-type semiconducting behavior as it possesses positive resistance change on reducing gas (ethanol) and negative change on oxidizing gas (NO_2). In both ethanol and NO_2, it is demonstrated that vertically aligned MoS_2 film with fully edge sites exposed shows significantly higher gas response than horizontally aligned films with basal plane exposed. That is, as a portion of vertically aligned MoS_2 region increases, response to the gas molecules drastically increases.

To further demonstrate highly enhanced gas adsorption properties in vertically aligned MoS_2 film, resistance variations of MoS_2 films to wide range of diluted NO_2 (0.1−100 ppm) gas are measured. Figure 4d shows the maximum amplitudes of electrical responses ($(\Delta R/R_b)_{max}$) for each synthesized MoS_2 films within the 0.1−100 ppm of NO_2 exposure period (10 min). It is clearly seen that vertically aligned MoS_2 films can detect 0.1 ppm of NO_2 with 0.2% of $(\Delta R/R_b)_{max}$, which is impossible to detect with horizontally aligned MoS_2. The significant enhancement of electrical resistance change in vertically aligned MoS_2 layers might be formed by highly enhanced gas adsorption capacity in edge sites of MoS_2. This highly enhanced gas adsorption properties in vertically aligned MoS_2 films is due to strong binding energy between NO_2 molecules and edge sites of vertically aligned MoS_2 layers originated from unique local stoichiometry differences from inert basal planes structure.[11] Accordingly, the edge sites exposed MoS_2 films can adsorb much larger number of NO_2

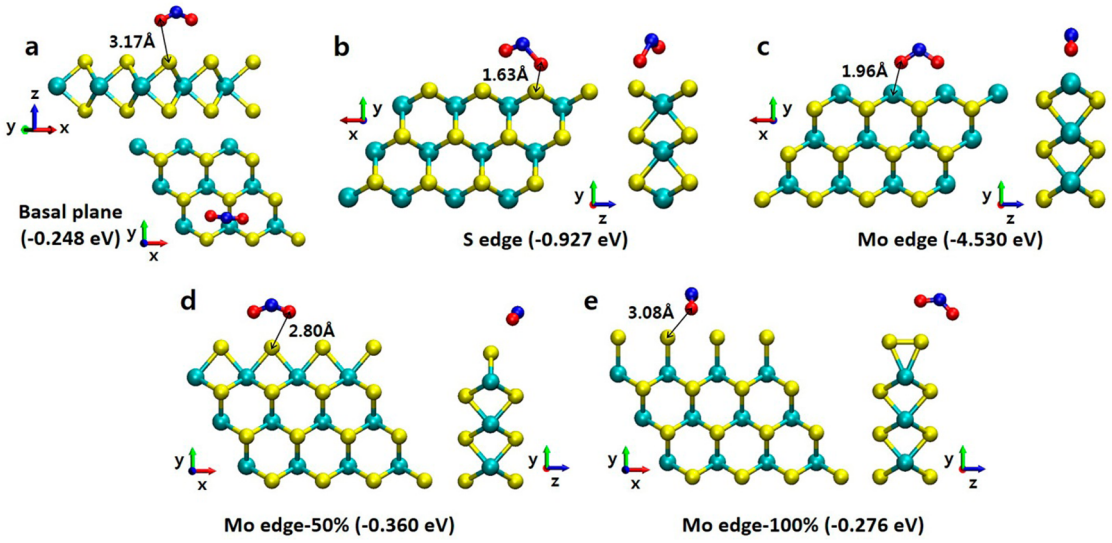

Figure 5. Snapshots of adsorbed NO_2 configurations on the (a) basal plane, (b) S edge, (c) Mo edge, (d) Mo edge-50% and (e) Mo edge-100%. The vacuum region extends along the *z*-direction for the basal plane case and along the *y*-direction for the edge cases. In rest of the directions, the MoS_2 atoms are fully periodic with two layers of Mo atoms separated by 6.28 Å (determined from DFT relaxation) along the *z* direction (only one layer of Mo atoms are shown and rest are truncated in the illustrations for visualization purposes). The minimum distance between NO_2 and MoS_2 and the binding energy values of NO_2 molecules are shown in the Figure. Cyan, red, yellow, and blue spheres represent molybdenum, oxygen, sulfur, and nitrogen, respectively.

molecules compared to basal plane exposed MoS_2 films which have low surface energy during identical exposure time even in same surface area exposed to gas molecules (Figure 4e).

To understand such distinct gas adsorption behaviors depending on the MoS_2 alignment, density functional theory (DFT) was conducted by computing the binding energies of NO_2 molecules in each MoS_2 layers. Because the Mo edge layer can be saturated with S atoms under certain conditions,[24,25] DFT calculations were extended to two different coverages of S (50 and 100%) on the Mo edge, along with the basal plane, Mo edge, and S edge. The configurations for 50 and 100% S coverage layers were taken from Seivane *et al.*[26] The aforementioned five systems were expanded into supercells to reduce the interactions between the periodic images of the NO_2 molecules with illustrations shown in Figure S4. The slab model was used with three MoS_2 layers (three horizontally aligned layers in basal plane calculations and three vertically aligned layers in edge calculations) in all of the calculations, which were sufficiently large to obtain convergent behavior for the NO_2 binding energy values. The snapshots of the NO_2 binding energy configurations near the different MoS_2 layers are shown in Figure 5. In the basal plane, S edge, Mo edge, Mo edge-50%, and Mo edge-100%, the computed binding energy values are −0.248, −0.927, −4.530, −0.360, and −0.276 eV, respectively. NO_2 binds stronger to the edge layers compared to the basal plane configuration, which is consistent with our experimental data showing superior adsorption properties along the edge layer. The distance between the NO_2 molecules and the Mo edge/S edge is relatively small (1.96 Å for Mo edge and 1.63 Å for S edge) as the oxygen atoms of NO_2 interacts strongly with the dangling bonds on the MoS_2 edge. The relatively large binding energy values computed along the Mo and the S edge layers are consistent with similar trends observed for LiS_2 in MoS_2.[18] Although the NO_2 binding weakens with the addition of S coverage (50% and 100%), it still remains stronger compared to the basal plane case. Given that it is difficult in practice to identify the precise atomic compositions along the edge layers, the fact that DFT calculations for varying configurations of the edge layers all lead to stronger NO_2 binding provides consistency between the computational and experimental results.

CONCLUSION

We report for the first time the comprehensive relationship between gas adsorption and MoS_2 alignment. We observe that gas response on NO_2 exposure of vertically aligned MoS_2 layers is about five times higher than that of horizontally aligned MoS_2 films during same exposure time. This is due to higher adsorption energy on MoS_2 edge as compared to basal plane of the MoS_2 films. To verify the superior gas sensing properties near the MoS_2 edge, the DFT calculations for multiple configurations of the edge layers were conducted and the computed NO_2 binding energies near the edge sites of MoS_2 are shown to be much stronger than those of basal plane of the MoS_2. We believe that our research provides not only first clear comparison study of gas adsorption properties between edge and terrace

sites of MoS_2, but also key factor for solving limitation of previous MoS_2 gas sensor mostly based on basal plane having low adsorption energy and active sites.

METHODS

MoS_2 Film Synthesis and Chemiresistors Fabrication. To synthesize MoS_2 films with various surface morphology, 1, 5, and 15 nm thick Mo seed layers are deposited onto SiO_2/Si substrate (300 nm SiO_2 thickness) with predetermined channel regions using e-beam evaporation process. The deposition rate was 0.1 Å/s. The Mo deposited SiO_2/Si substrate was placed at central furnace and quartz tube containing elemental sulfur powders (4 g, from Sigma-Aldrich) was placed at the upstream furnace carefully. The tube is pumped to a base pressure of 10 mTorr and flushed with 50 sccm of Ar gas to remove residue oxygen. When 50 sccm of Ar gas is injected, pressure of CVD furnace is maintained with 0.7 Torr during the reaction. The central furnace is quickly raised to reaction temperature of 770 °C within 20 min first, and the upstream furnace locating sulfur powder is raised to 220 °C within 5 min. Then, the furnace is held at reaction temperature for 30 min, followed by natural cool-down, during Ar flushing. Schematic illustration of the rapid sulfurization mechanism and CVD instrument is shown in Figure S1a,b.

Morphological Characterizations. The surface morphology of the synthesized MoS_2 films was characterized with optical microscopy (LV-100POL, Nikon), AFM (Park Systems, XE-100), X-ray diffractometer (RIGAKU, D/MAX-2500), Raman spectroscopy (Horiba Jobin Yvon ARAMIS), and TEM (Philips Technical F30). For TEM sample preparation, poly(methyl methacrylate) (PMMA, Sigma-Aldrich) was coated on synthesized MoS_2 films on SiO_2/Si substrates. After thermal annealing of 180 °C for 5 min, substrates were immersed in potassium hydroxide (KOH) solution for selective etching of SiO_2. Once the PMMA/MoS_2 films were lifted off, they were transferred to Ni TEM grid and washed with acetone to remove PMMA residue.

Measurement of the Resistance Signal of the MoS_2 Films. With synthesized MoS_2 films, 70 nm thick Au electrodes (5 nm Ti was predeposited as an adhesion layer) with 100 μm spacing and width were deposited by e-beam evaporation with a customized SERS mask to measure the resistance signal of the MoS_2 channel. The sensors were mounted on a sensing chamber designed to measure the resistance signal by a data acquisition module (Agilent 34970A), while the controlled ethanol and NO_2 gas were passed through the sensing chamber. A self-designed gas delivery system was also used to control the gas flow into the sensing chamber, in order to measure the sensor response of the analytes. The test analytes used in this study were a N2 based 1000 ppm ethanol and 100 ppm of NO_2 gas. A serial dilution system used to control the NO_2 concentration was designed using a MFC (mass flow controller, Brooks 5850E), Teflon tubing (PFA, 1/8 in.), LOK type fitting, and a valve system. Schematic illustration of the chemiresistor fabrication process and gas delivery system is shown in Figures S1c and S2, respectively.

Theoretical Calculations Using DFT. All of the DFT simulations were performed using the Quantum-ESPRESSO package.[27] The generalized gradient approximation (GGA) functional of Perdew, Burke, and Ernzerhof (PBE) was adopted to express the exchange correlation terms,[28] and DFT-d2 was used for the vdW functionals as PBE cannot describe vdW interactions accurately.[29] Large vacuum distance (*i.e.*, more than 15 Å) was imposed in the slab model to avoid unwanted interlayer interactions. The 4 × 4 × 1 Monkhorst−Pack k-points were used,[30] and the plane wave energy cutoff was set to 680 eV.

Conflict of Interest: The authors declare no competing financial interest.

Supporting Information Available: The Supporting Information is available free of charge on the ACS Publications website at DOI: 10.1021/acsnano.5b04504.

Schematic illustration of CVD constructions and *v*, schematic diagram of overall gas delivery and resistance measurement systems, AFM profiles of vertically aligned and horizontally aligned MoS*2* films, DFT calculation method (PDF)

Acknowledgment. H.-T. Jung acknowledges the financial support by National Research Foundation of Korea (NRF), funded by the Ministry of Science, ICT, and Future Planning, Korea (MISP, Grant No. 2015R1A2A1A05001844), Global Frontier Research Center for Advanced Soft Electronics (No. 2014M3A6A5060937, MISP), and the Climate Change Research Hub of KAIST (No. N01150139). J. Kim and Y. Lee were supported by Basic Science Research Program through the National Research Foundation of Korea (NRF) funded by the Ministry of Education (2014R1A1A2055853).

REFERENCES AND NOTES

1. Wang, Q. H.; Kalantar-Zadeh, K.; Kis, A.; Coleman, J. N.; Strano, M. S. Electronics and Optoelectronics of Two-Dimensional Transition Metal Dichalcogenides. *Nat. Nanotechnol.* **2012**, *7*, 699–712.
2. Chhowalla, M.; Shin, H. S.; Eda, G.; Li, L.-J.; Loh, K. P.; Zhang, H. The Chemistry of Two-Dimensional Layered Transition Metal Dichalcogenide Nanosheets. *Nat. Chem.* **2013**, *5*, 263–275.
3. Kibsgaard, J.; Chen, Z.; Reinecke, B. N.; Jaramillo, T. F. Engineering the Surface Structure of MoS_2 to Preferentially Expose Active Edge Sites for Electrocatalysis. *Nat. Mater.* **2012**, *11*, 963–969.
4. Radisavljevic, B.; Radenovic, A.; Brivio, J.; Giacometti, V.; Kis, A. Single-Layer MoS_2 Transistors. *Nat. Nanotechnol.* **2011**, *6*, 147–150.
5. Lopez-Sanchez, O.; Lembke, D.; Kayci, M.; Radenovic, A.; Kis, A. Ultrasensitive Photodetectors Based on Monolayer MoS_2. *Nat. Nanotechnol.* **2013**, *8*, 497–501.
6. Zhu, C.; Zeng, Z.; Li, H.; Li, F.; Fan, C.; Zhang, H. Single-Layer MoS_2-Based Nanoprobes for Homogeneous Detection of Biomolecules. *J. Am. Chem. Soc.* **2013**, *135*, 5998–6001D.
7. Kim, J.-S.; Yoo, H.-W.; Choi, H. O.; Jung, H.-T. Tunable Volatile Organic Compounds Sensor by Using Thiolated Ligand Conjugation on MoS_2. *Nano Lett.* **2014**, *14*, 5941–5947.
8. Perkins, F. K.; Friedman, A. L.; Cobas, E.; Campbell, P. M.; Jernigan, G. G.; Jonker, B. T. Chemical Vapor Sensing with Monolayer MoS_2. *Nano Lett.* **2013**, *13*, 668–673.
9. Lee, K.; Gatensby, R.; McEvoy, N.; Hallam, T.; Duesberg, G. S. High-Performance Sensors Based on Molybdenum Disulfide Thin Films. *Adv. Mater.* **2013**, *25*, 6699–6702.
10. Late, D. J.; Huang, Y.-K.; Liu, B.; Acharya, J.; Shirodkar, S. N.; Luo, J.; Yan, A.; Charles, D.; Waghmare, U. V.; Dravid, V. P.; Rao, C. N. R. Sensing Behavior of Atomically Thin-Layered MoS_2 Transistors. *ACS Nano* **2013**, *7*, 4879–4891.
11. Jaramillo, T. F.; Jørgensen, K. P.; Bonde, J.; Nielsen, J. H.; Horch, S.; Chorkendorff, I. Identification of Active Edge Sites for Electrochemical H_2 Evolution from MoS_2 Nanocatalysts. *Science* **2007**, *317*, 100–102.
12. Remškar, M.; Iskra, I.; Jelenc, J.; Škapin, S. D.; Višić, B.; Varlec, A.; Kržan, A. A Novel Structure of Polyvinylidene Fluoride (PVDF) Stabilized by MoS_2 Nanotubes. *Soft Matter* **2013**, *9*, 8647–8653.
13. Lei, B.; Li, G. R.; Gao, X. P. Morphology Dependence of Molybdenum Disulfide Transparent Counter Electrode in Dye-Sensitized Solar Cells. *J. Mater. Chem. A* **2014**, *2*, 3919–3925.
14. Yang, Y.; Fei, H.; Ruan, G.; Xiang, C.; Tour, J. M. Edge-Oriented MoS_2 Nanoporous Films as Flexible Electrodes for Hydrogen Evolution Reactions and Supercapacitor Devices. *Adv. Mater.* **2014**, *26*, 8163–8168.

15. Kong, D.; Wang, H.; Cha, J. J.; Pasta, M.; Koski, K. J.; Yao, J.; Cui, Y. Synthesis of MoS_2 and $MoSe_2$ Films with Vertically Aligned Layers. *Nano Lett.* **2013**, *13*, 1341–1347.
16. Wang, H.; Lu, Z.; Kong, D.; Sun, J.; Hymel, T. M.; Cui, Y. Electrochemical Tuning of MoS_2 Nanoparticles on Three-Dimensional Substrate for Efficient Hydrogen Evolution. *ACS Nano* **2014**, *8*, 4940–4947.
17. Gao, M.-R.; Chan, M. K. Y.; Sun, Y. Edge-Terminated Molybdenum Disulfide with a 9.4Å Interlayer Spacing for Electrochemical Hydrogen Production. *Nat. Commun.* **2015**, *6*, 7493.
18. Wang, H.; Zhang, Q.; Yao, H.; Liang, Z.; Lee, H.-W.; Hsu, P.-C.; Zheng, G.; Cui, Y. High Electrochemical Selectivity of Edge *versus* Terrace Sites in Two-Dimensional Layered MoS_2 Materials. *Nano Lett.* **2014**, *14*, 7138–7144.
19. Asadi, M.; Kumar, B.; Behranginia, A.; Rosen, B. A.; Baskin, A.; Repnin, N.; Pisasale, D.; Phillips, P.; Zhu, W.; Haasch, R.; et al. Robust Carbon Dioxide Reduction on Molybdenum Disulphide Edges. *Nat. Commun.* **2014**, 10.1038/ncomms5470.
20. Gaur, A. P. S.; Sahoo, S.; Ahmadi, M.; Dash, S. P.; Guinel, M. J.-F.; Katiyar, R. S. Surface Energy Engineering for Tunable Wettability Through Controlled Synthesis of MoS_2. *Nano Lett.* **2014**, *14*, 4314–4321.
21. Yin, X.; Ye, Z.; Chenet, D. A.; Ye, Y.; O'Brien, K.; Hone, J. C.; Zhang, X. Edge Nonlinear Optics on a MoS_2 Atomic Monolayer. *Science* **2014**, *344*, 488–490.
22. Jung, Y.; Shen, J.; Liu, Y.; Woods, J. M.; Sun, Y.; Cha, J. J. Metal Seed Layer Thickness-Induced Transition from Vertical to Horizontal Growth of MoS_2 and WS_2. *Nano Lett.* **2014**, *14*, 6842–6849.
23. Lee, C.; Yan, H.; Brus, L. E.; Heinz, T. F.; Hone, J.; Ryu, S. Anomalous Lattice Vibrations of Single- and Few-layer MoS_2. *ACS Nano* **2010**, *4*, 2695–2700.
24. Lauritsen, J. V.; Kibsgaard, J.; Helveg, S.; Topsøe, H.; Clausen, B. S.; Laegsgaard, E.; Besenbacher, F. Size-Dependent Structure of MoS_2 Nanocrystals. *Nat. Nanotechnol.* **2007**, *2*, 53–58.
25. Bollinger, M.; Jacobsen, K.; Nørskov, J. Atomic and Electronic Structure of MoS_2 Nanoparticles. *Phys. Rev. B: Condens. Matter Mater. Phys.* **2003**, *67*, 085410.
26. Seivane, L. F.; Barron, H.; Botti, S.; Lopes Marques, M. A.; Rubio, Á.; López-Lozano, X. Atomic and Electronic Properties of Quasi-One-Dimensional MoS_2 Nanowires. *J. Mater. Res.* **2013**, *28*, 240–249.
27. Giannozzi, P.; Baroni, S.; Bonini, N.; Calandra, M.; Car, R.; Cavazzoni, C.; Ceresoli, D.; Chiarotti, G. L.; Cococcioni, M.; Dabo, I. QUANTUM ESPRESSO: A Modular and Open-Source Software Project for Quantum Simulations of Materials. *J. Phys.: Condens. Matter* **2009**, *21*, 395502.
28. Perdew, J. P.; Burke, K.; Ernzerhof, M. J. Generalized Gradient Approximation Made Simple. *Phys. Rev. Lett.* **1996**, *77*, 3865–3868.
29. Grimme, S.; Antony, J.; Ehrlich, S.; Krieg, H. A Consistent and Accurate Ab Initio Parametrization of Density Functional Dispersion Correction (DFT-D) for the 94 Elements H-Pu. *J. Chem. Phys.* **2010**, *132*, 154104.
30. Pack, J. D.; Monkhorst, H. J. "Special Points for Brillouin-Zone Integrations" —a reply*. *Phys. Rev. B* **1977**, *16*, 1748–1749.